ELSEVIER

Comput. Methods Appl. Mech. Engrg. 130 (1996) 57–79

Computer methods in applied mechanics and engineering

A 4-node finite shell element for the implementation of general hyperelastic 3D-elasticity at finite strains

P. Betsch, F. Gruttmann, E. Stein*

Institut für Baumechanik und Numerische Mechanik, Universität Hannover, Appelstraße 9A, 30167 Hannover, Germany

Received 5 July 1994; revised 15 May 1995

Abstract

In this paper a finite shell element for large deformations is presented based on extensible director kinematics. The essential feature is an interface to arbitrary three-dimensional material laws. The non-linear Lagrangian formulation is based on the three-field variational principle, parametrized with the displacement vector, enhanced Green–Lagrangian strain tensor and second Piola Kirchhoff stress tensor. The developed quadrilateral shell element is characterized by a coarse mesh accuracy and distortion insensitivity compared with bilinear displacement approaches. Furthermore, plane stress response is approximately recovered in the asymptotic case of vanishing thickness. A number of example problems investigating large deformation as well as finite strain applications are presented. Compressible and incompressible hyperelastic materials of the St. Venant-Kirchhoff, Neo-Hookean and Mooney–Rivlin type are particularly used.

1. Introduction

Shell elements are mainly developed within the context of the so-called *degenerated approach* and on the other hand, the *classical shell theory*. The kinematic assumption underlying the variational formulation are essentially the same for both formulations however the reduction to stress resultants is carried out numerically in the former and analytically in the latter.

Common assumptions in many shell theories are inextensibility in thickness direction and the zero normal stress condition. Therefore, the three-dimensional constitutive equations are usually modified by incorporating the plane stress condition. This approach has been applied within the finite element method in several publications (see e.g. [1–8] among many others). In this context a lot of research has been spent on the investigation of a convenient description of finite rotations. The constitutive response is usually restricted to the St. Venant-Kirchhoff material which is only valid for small strains.

Large strains have been considered in different publications. In [9] the plane stress condition yields the thickness change in the context of large membrane strains. Parisch [10] and Schieck et al. [11] deal with incompressible (rubber-like) materials where the incompressibility condition is used to determine the thickness of the deformed shell as dependent variable of the in-plane strains. There the theory is restricted to incompressibility only. Furthermore, the constitutive equations are modified by an independent static hypothesis concerning the approximately plane stress condition.

*Corresponding author.

SSDI 0045-7825(95)00920-5

In general, large strain constitutive algorithms under the plane stress constraint are very cumbersome and in the most cases not available. Therefore, our interest is the presentation of a robust shell element for large deformations with an interface to general hyperelastic three-dimensional material laws. We make use of an extensible director formulation which avoids the explicit enforcement of the plane stress constraint.

Dropping the inextensibility constraint permits a kinematic description without rotation tensor as in continuum mechanics (see e.g. [12–14]). However, the direct bilinear interpolation of the extensible director field yields poor performance of the discrete model in the thin-shell limit and thus is only suitable for the calculation of thick shells, as has been shown by Simo et al. [15]. Therefore, in [15] a multiplicative decomposition of the director field into an extensible and inextensible part has been proposed. Thereby, the shell theory in [15] contains nonstandard strain measures and work conjugate 'modified effective stress resultants'.

Contrary to [15] our proposed continuum based approach relies directly on the Second Piola–Kirchhoff stress tensor and the work conjugate Green–Lagrangian strain tensor. Despite the same parametrization of the extensible director field as in [15], the discretization of the covariant Green–Lagrangian strains now leads directly to the interpolation of the thickness stretch along with a simple additive update formula. Accordingly, the thickness stretch is included within the interpolation constants of the generalized finite element displacement vector.

The resulting finite shell element is developed within the degenerated concept where the intrinsic through-the-thickness integration accounts naturally for non-linear material behaviour. For this reason the crucial question of a proper description of 2D-constitutive equations at finite strains, as done in [16, 17] or [11], is circumvented within the numerical (degenerated) approach. That means that no shell-specific approximations of the three-dimensional constitutive equations are incorporated.

On the other hand, as a consequence of the unmodified 3D-constitutive laws we now need at least linearly varying transverse normal strains over the shell thickness. To achieve this we make use of the enhanced assumed strain method developed in [18, 19], which for the present purpose was proposed by Büchter et al. [14] in order to obtain a linear distribution of the transverse normal strains.

We further use the enhanced assumed strain method to enhance the tangential strains in order to improve the performance in coarse meshes, particularly in bending dominated situations and in the incompressible limit. Therefore, we present an expansion of the enhanced tangential strains which accounts for the covariant strain formulation in a natural way. Compared with other mixed shell elements [4, 15] (partially) based on the Hellinger–Reissner formulation the advantage of the present assumed strain shell element is to be seen in the treatment of general 3D-constitutive equations which is identical to that arising in the displacement based approach.

Some features of the present formulation are summarized as follows:

(i) The developed degenerated shell element is formulated in convected coordinates, applying covariant Green–Lagrangian strains, without neglecting any higher order terms. We make use of extensible director kinematics which allow for homogeneous extensibility and therefore constant transverse normal strains. Thus the theory accounts for all stress and strain components of the three-dimensional constitutive equations.

(ii) In the presented paper an interface to three-dimensional hyperelastic material laws is given. No shell specific modifications are necessary to implement non-linear material laws with compressible and incompressible behaviour.

(iii) The non-linear Lagrangian formulation is based on the three-field variational principle, parametrized with the displacement vector, enhanced Green–Lagrangian strain tensor and Second Piola–Kirchhoff stress tensor. This is in contrast to the work of Simo and Armero [19], where the material displacement gradient has been enhanced within a spatial formulation.

(iv) The developed quadrilateral shell element shows the same coarse mesh accuracy and distortion insensitivity as stress-based mixed Hellinger–Reissner formulations. The present mixed formulation has not to be modified for physical non-linear response as for rubberlike materials or materials undergoing large elasto-plastic deformations.

(v) The present formulation allows for both: the discretization of smooth shell surfaces as well as folded shell structures. Other extensible shell formulations, see for example [12] or [14], do not offer this possibility because there rotational degrees of freedom are not used.

The paper concludes with a number of example problems where large deformation as well as finite strain applications are investigated within the case of compressible and incompressible elasticity. Several linear and non-linear examples show that in the asymptotic case of vanishing thickness plane stress response is recovered. Particularly, three-dimensional hyperelastic constitutive models of the St. Venant-Kirchhoff, Neo-Hookean and Mooney–Rivlin type are investigated. Comparisons of our results are made if possible with those reported in the literature.

2. Shell kinematics

Let $\mathcal{B}_0$ be the region of three-dimensional Euclidean space occupied by the shell in the reference configuration with boundary $\partial\mathcal{B}_0$. The position vector $\boldsymbol{X}$ of any point $P \in \mathcal{B}_0$ is defined by

$$\begin{aligned} &\boldsymbol{X}(\xi^1,\xi^2,\xi^3) = X^i\boldsymbol{e}_i = \boldsymbol{\Phi}(\xi^1,\xi^2) + \xi^3\boldsymbol{D}(\xi^1,\xi^2) \\ &\quad \text{with } |\boldsymbol{D}(\xi^1,\xi^2)| = 1 \quad \text{and} \quad -\frac{h_0}{2} \leqslant \xi^3 \leqslant \frac{h_0}{2} \end{aligned} \tag{1}$$

where $\boldsymbol{\Phi}(\xi^1,\xi^2)$ denotes a configuration of the reference shell mid-surface $\mathcal{M}_0$. With (ξ^i) and $(\boldsymbol{e}_i)$ we denote a material (convected) coordinate system of the body and a system of orthonormal vectors that forms the global triad, respectively. A director $\boldsymbol{D}(\xi^1,\xi^2)$ is defined as a vector collinear with the transverse fiber and perpendicular to the shell mid-surface $\mathcal{M}_0$. Throughout this paper the usual summation convention is used where Latin indices range from 1 to 3 and Greek indices range from 1 to 2. The geometry of the deformed shell space $\mathcal{B}$ is described by the position vector

$$\boldsymbol{x}(\xi^1,\xi^2,\xi^3) = x^i\boldsymbol{e}_i = \boldsymbol{\varphi}(\xi^1,\xi^2) + \xi^3\boldsymbol{d}(\xi^1,\xi^2). \tag{2}$$

The extensible director $\boldsymbol{d}(\xi^1,\xi^2)$ accounts for deformation dependent thickness change and allows for transverse shear strains to occur. Furthermore, $\boldsymbol{\varphi}(\xi^1,\xi^2)$ denotes the position vector of the actual shell mid-surface $\mathcal{M}$. We introduce a multiplicative decomposition of the director field into an inextensible vector part and a scalar stretching part [15]

$$\boldsymbol{d}(\xi^1,\xi^2) = \lambda(\xi^1,\xi^2)\boldsymbol{t}(\xi^1,\xi^2) \quad \text{with} \quad |\boldsymbol{t}(\xi^1,\xi^2)| = 1 \quad \text{and} \quad \lambda = h/h_0 > 0. \tag{3}$$

The thickness stretch $\lambda(\xi^1,\xi^2)$ accounts for thickness changes in the direction of the rotated unit director $\boldsymbol{t} = \boldsymbol{R}\boldsymbol{D}$, where $\boldsymbol{R}$ denotes an orthogonal tensor. The displacement in the shell can now be calculated from $\boldsymbol{u} = \boldsymbol{x} - \boldsymbol{X}$ and leads to

$$\boldsymbol{u}(\xi^1,\xi^2,\xi^3) = \boldsymbol{\varphi}(\xi^1,\xi^2) - \boldsymbol{\Phi}(\xi^1,\xi^2) + \xi^3\left[\lambda(\xi^1,\xi^2)\boldsymbol{R}(\xi^1,\xi^2) - \mathbf{1}\right]\boldsymbol{D}(\xi^1,\xi^2). \tag{4}$$

In the following, all quantities defined with respect to $\mathcal{B}_0$ are denoted by capital letters and by lower case letters when referred to $\mathcal{B}$. The tangent vectors $\boldsymbol{g}_i$ and $\boldsymbol{G}_i$ to the coordinate line ξ^i are given by

$$\boldsymbol{G}_i = G_i^I\boldsymbol{e}_I = \frac{\partial\boldsymbol{X}}{\partial\xi^i}, \qquad \boldsymbol{g}_i = g_i^I\boldsymbol{e}_I = \frac{\partial\boldsymbol{x}}{\partial\xi^i}. \tag{5}$$

Introducing shell kinematics (1) and (2) yields the covariant base vectors

$$\boldsymbol{G}_\alpha = \frac{\partial\boldsymbol{\Phi}}{\partial\xi^\alpha} + \xi^3\frac{\partial\boldsymbol{D}}{\partial\xi^\alpha}, \qquad \boldsymbol{G}_3 = \boldsymbol{D}, \tag{6}$$

$$\boldsymbol{g}_\alpha = \frac{\partial\boldsymbol{\varphi}}{\partial\xi^\alpha} + \xi^3\frac{\partial\boldsymbol{d}}{\partial\xi^\alpha}, \qquad \boldsymbol{g}_3 = \boldsymbol{d}. \tag{7}$$

The deformation gradient relates the base vectors of the reference configuration to the base vectors of the deformed configuration:

$$\boldsymbol{F} = \operatorname{Grad}\boldsymbol{x} = \boldsymbol{g}_i \otimes \boldsymbol{G}^i, \qquad \boldsymbol{g}_i = \boldsymbol{F}\boldsymbol{G}_i, \qquad \boldsymbol{g}^i = \boldsymbol{F}^{-T}\boldsymbol{G}^i, \tag{8}$$

where the contravariant base vectors $\boldsymbol{G}^i$ und $\boldsymbol{g}^i$ are defined by

$$\boldsymbol{g}_i \cdot \boldsymbol{g}^j = \delta_i^j, \qquad \boldsymbol{G}_i \cdot \boldsymbol{G}^j = \delta_i^j. \tag{9}$$

We describe the state of deformation by means of Green–Lagrangian strain tensor

$$\boldsymbol{E} = \frac{1}{2}\left(\boldsymbol{F}^{\mathrm{T}}\boldsymbol{F} - \boldsymbol{1}\right) = E_{ij}\boldsymbol{G}^{i} \otimes \boldsymbol{G}^{j}, \tag{10}$$

where the covariant components of $\boldsymbol{E}$ read

$$E_{ij} = \frac{1}{2}(g_{ij} - G_{ij}), \tag{11}$$

with the covariant components of the metric tensor defined by

$$G_{ij} = \boldsymbol{G}_{i} \cdot \boldsymbol{G}_{j}, \qquad g_{ij} = \boldsymbol{g}_{i} \cdot \boldsymbol{g}_{j}. \tag{12}$$

We further obtain

$$G = \det[G_{ij}], \qquad g = \det[g_{ij}], \qquad \mathrm{d}V = \sqrt{G}\,\mathrm{d}\xi^{1}\,\mathrm{d}\xi^{2}\,\mathrm{d}\xi^{3}, \qquad J = \det \boldsymbol{F} = \sqrt{g/G}. \tag{13}$$

Applying shell kinematics (2) to the covariant components of the metric tensor $(12)_2$ and with the abbreviation $(\,)_{,\alpha} = \partial/\partial\xi^{\alpha}(\,)$ for partial differentiation one obtains

$$\begin{aligned} g_{\alpha\beta} &= \boldsymbol{\varphi}_{,\alpha} \cdot \boldsymbol{\varphi}_{,\beta} + \xi^{3}[\boldsymbol{d}_{,\alpha} \cdot \boldsymbol{\varphi}_{,\beta} + \boldsymbol{\varphi}_{,\alpha} \cdot \boldsymbol{d}_{,\beta}] + (\xi^{3})^{2}\boldsymbol{d}_{,\alpha} \cdot \boldsymbol{d}_{,\beta} \\ g_{\alpha 3} &= \boldsymbol{\varphi}_{,\alpha} \cdot \boldsymbol{d} + \xi^{3}\boldsymbol{d} \cdot \boldsymbol{d}_{,\alpha} \\ g_{33} &= \boldsymbol{d} \cdot \boldsymbol{d} \end{aligned} \tag{14}$$

along with analogous expressions for $G_{\alpha\beta}$, $G_{\alpha 3}$ and G_{33}. Incorporating the multiplicative decomposition of the extensible director field (3) yields the reparametrized representation

$$\begin{aligned} g_{\alpha\beta} &= \boldsymbol{\varphi}_{,\alpha} \cdot \boldsymbol{\varphi}_{,\beta} + \xi^{3}[\lambda(\boldsymbol{t}_{,\alpha} \cdot \boldsymbol{\varphi}_{,\beta} + \boldsymbol{\varphi}_{,\alpha} \cdot \boldsymbol{t}_{,\beta}) + (\lambda_{,\alpha}\boldsymbol{\varphi}_{,\beta} + \boldsymbol{\varphi}_{,\alpha}\lambda_{,\beta}) \cdot \boldsymbol{t}] + (\xi^{3})^{2}[\lambda_{,\alpha}\lambda_{,\beta} + \lambda^{2}\boldsymbol{t}_{,\alpha} \cdot \boldsymbol{t}_{,\beta}] \\ g_{\alpha 3} &= \lambda\boldsymbol{\varphi}_{,\alpha} \cdot \boldsymbol{t} + \xi^{3}\lambda\lambda_{,\alpha} \\ g_{33} &= \lambda^{2} \end{aligned} \tag{15}$$

According to this the covariant components of the Green–Lagrangian strain tensor are given by

$$E_{\alpha\beta} = \frac{1}{2}(g_{\alpha\beta} - G_{\alpha\beta}), \qquad E_{\alpha 3} = \frac{1}{2}(g_{\alpha 3} - G_{\alpha 3}), \qquad E_{33} = \frac{1}{2}(\lambda^{2} - 1) \tag{16}$$

with tangential strains $E_{\alpha\beta}$, transverse shear strains $E_{\alpha 3}$ and thickness strains E_{33}.

3. Variational formulation

In this section we present an extension of the enhanced assumed strain method of Simo and Rifai [18] to the finite deformation case within a Lagrangian setting. The governing variational equations of the enhanced assumed strain method can be derived from a Hu–Washizu variational principle in combination with a reparametrization of the strain fields. Within a Lagrangian shell formulation we consider a strain field of the form

$$\boldsymbol{E} = \boldsymbol{E}^{C} + \tilde{\boldsymbol{E}} \tag{17}$$

where $\boldsymbol{E}^{C}$ is the Green–Lagrangian strain tensor compatible to the displacement field $\boldsymbol{u}$

$$\boldsymbol{E}^{C} = \frac{1}{2}\left(\mathrm{Grad}\,\boldsymbol{u}^{\mathrm{T}} + \mathrm{Grad}\,\boldsymbol{u} + \mathrm{Grad}\,\boldsymbol{u}^{\mathrm{T}}\,\mathrm{Grad}\,\boldsymbol{u}\right) \tag{18}$$

and $\tilde{\boldsymbol{E}}$ denotes the enhanced part of the strain field, which in the finite element context is intended to enhance the thickness strains $(16)_3$ and the tangential strains $(16)_1$. The present parametrization is in contrast to the work of Simo and Armero [19] where in the context of finite deformations a spatial formulation has been employed and the displacement gradient has been enhanced. The modified three-field variational principle now reads

$$\tilde{\Pi}\left(\boldsymbol{u},\tilde{\boldsymbol{E}},\boldsymbol{S}\right)=\int_{\mathcal{B}_0}\left[\hat{W}_{0s}(\boldsymbol{E}^C+\tilde{\boldsymbol{E}})-\boldsymbol{S}\cdot\tilde{\boldsymbol{E}}\right]\mathrm{d}V+\Pi_{\mathrm{ext}}(\boldsymbol{u}) \tag{19}$$

so that the displacements $\boldsymbol{u}$, the enhanced Green–Lagrangian strain tensor $\tilde{\boldsymbol{E}}$ and the work conjugate Second Piola–Kirchhoff stress tensor $\boldsymbol{S}$ are treated as independent variables. $\hat{W}_{0s}$ denotes the strain energy density function per unit initial volume and Π_{ext} is the potential of the conservative external forces

$$\Pi_{\mathrm{ext}}(\boldsymbol{u})=-\int_{\mathcal{B}_0}\varrho_0\bar{\boldsymbol{b}}\cdot\boldsymbol{u}\,\mathrm{d}V-\int_{\partial\mathcal{B}_{0\sigma}}\bar{\boldsymbol{t}}\cdot\boldsymbol{u}\,\mathrm{d}A \tag{20}$$

where $\bar{\boldsymbol{b}}$ and $\bar{\boldsymbol{t}}$ are applied body forces and surface forces, respectively. Variation of (19) with respect to the independent variables yields the weak form of the boundary value problem

$$\int_{\mathcal{B}_0}\frac{\partial\hat{W}_{0s}}{\partial\boldsymbol{E}}\cdot\left(\delta\boldsymbol{E}^C+\delta\tilde{\boldsymbol{E}}\right)\mathrm{d}V-\underline{\int_{\mathcal{B}_0}\boldsymbol{S}\cdot\delta\tilde{\boldsymbol{E}}\,\mathrm{d}V}=\int_{\mathcal{B}_0}\varrho_0\bar{\boldsymbol{b}}\cdot\delta\boldsymbol{u}\,\mathrm{d}V+\int_{\partial\mathcal{B}_{0\sigma}}\bar{\boldsymbol{t}}\cdot\delta\boldsymbol{u}\,\mathrm{d}A\underline{\int_{\mathcal{B}_0}\delta\boldsymbol{S}\cdot\tilde{\boldsymbol{E}}\,\mathrm{d}V}=0 \tag{21}$$

where $\delta\boldsymbol{E}^C$ denotes the variation of the compatible Green–Lagrangian strain tensor (18)

$$\delta\boldsymbol{E}^C=\mathrm{sym}\left(\mathrm{Grad}\,\delta\boldsymbol{u}^{\mathrm{T}}(\boldsymbol{1}+\mathrm{Grad}\,\boldsymbol{u})\right)\,. \tag{22}$$

If in the finite element context the approximation for the discontinuous enhanced strains are orthogonal to at least constant stress fields, then the underlined terms in (21) drop out and a two-field variational formulation remains. The orthogonality condition plays a central role in the stability analysis of the enhanced strain method, as has been shown in [18, 20] within the linear theory.

For the sake of completeness the local Euler–Lagrange equations associated with (21) can be obtained by standard arguments and yield the following equilibrium equations in $\mathcal{B}_0$ along with the stress boundary condition on $\partial\mathcal{B}_{0t}$

$$\left.\begin{aligned}&\mathrm{Div}[(\boldsymbol{1}+\mathrm{Grad}\,\boldsymbol{u})\boldsymbol{S}]+\varrho_0\bar{\boldsymbol{b}}=\boldsymbol{0}\\&\boldsymbol{S}=\frac{\partial\hat{W}_{0s}}{\partial\boldsymbol{E}}\\&\tilde{\boldsymbol{E}}=\boldsymbol{0}\end{aligned}\right\}\quad\text{in }\mathcal{B}_0$$

$$\bar{\boldsymbol{t}}=(\boldsymbol{F}\boldsymbol{S})\boldsymbol{N}\qquad\text{on }\partial\mathcal{B}_{0t} \tag{23}$$

4. Finite element approximation

In this section we describe the finite element approximation associated with the continuum weak form (21). We introduce a general finite element discretization $\mathcal{B}^h=\mathbf{A}_{e=1}^{n_{\mathrm{elem}}}\mathcal{B}_e$ with n_{elem} quadrilateral elements, where $\mathbf{A}$ denotes the standard assembly operator.

4.1. Compatible finite element interpolations

According to the isoparametric concept, the following geometric and kinematic variables are interpolated with the standard bilinear shape functions

$$N^I(\xi,\eta)=\frac{1}{4}\left(1+\xi\xi^I\right)\left(1+\eta\eta^I\right)\,. \tag{24}$$

Within a single element $\mathcal{B}_e$ the position vector of the reference mid-surface $\mathcal{M}_0^h$ and the deformed mid-surface $\mathcal{M}^h$ are approximated by

$$\boldsymbol{\Phi}(\xi,\eta)=\sum_{I=1}^{4}N^I(\xi,\eta)\boldsymbol{\Phi}_I\,,\qquad\boldsymbol{\varphi}(\xi,\eta)=\sum_{I=1}^{4}N^I(\xi,\eta)\boldsymbol{\varphi}_I\,. \tag{25}$$

The interpolation of the reference director field is performed as proposed in [4]

$$\boldsymbol{D} = \frac{\bar{\boldsymbol{D}}}{|\bar{\boldsymbol{D}}|}, \qquad \boldsymbol{D}_{,\alpha} = \frac{1}{|\bar{\boldsymbol{D}}|}(\mathbf{1} - \boldsymbol{D} \otimes \boldsymbol{D})\bar{\boldsymbol{D}}_{,\alpha} \quad \text{where } \bar{\boldsymbol{D}} = \sum_{I=1}^{4} N^I(\xi, \eta)\boldsymbol{D}_I \tag{26}$$

so that the unit length condition $|\boldsymbol{D}| = 1$ holds throughout the element.

Our description of finite rotations with two or three degrees of freedom is closely related to previous works of Hughes and Liu [21] and Simo et al. [4, 22]. In what follows, the symbols Δ and δ denote an increment and variation of the appropriate quantity. Furthermore, a superscript (k) denotes the iteration counter.

In the case of smooth shell mid-surfaces the singularity due to the in-plane rotation $\Delta\boldsymbol{\theta} = k \cdot \boldsymbol{t}$ ($k \in \mathbb{R}$) has to be eliminated. For that reason a unit local Cartesian (fiber) coordinate system is defined at each node with base vectors $\boldsymbol{a}_1^{(k)}, \boldsymbol{a}_2^{(k)}, \boldsymbol{a}_3^{(k)} = \boldsymbol{t}_I^{(k)}$ ordered in an orthogonal nodal matrix $\boldsymbol{\Lambda}_I^{(k)} = [\boldsymbol{a}_1, \boldsymbol{a}_2, \boldsymbol{t}]_I^{(k)}$. This fiber coordinate system is used as a reference frame for the incremental nodal unit director displacements $\Delta\boldsymbol{t}_I = \Delta T_{I1}\boldsymbol{a}_1 + \Delta T_{I2}\boldsymbol{a}_2$, so that the following relationships hold

$$\boldsymbol{t}_I^{(k)} = \boldsymbol{\Lambda}_I^{(k)}\boldsymbol{e}_3, \qquad \Delta\boldsymbol{t}_I = \boldsymbol{\Lambda}_I^{(k)}(\Delta T_{I1}\boldsymbol{e}_1 + \Delta T_{I2}\boldsymbol{e}_2), \qquad \Delta\boldsymbol{\theta}_I = \boldsymbol{t}_I^{(k)} \times \Delta\boldsymbol{t}_I \tag{27}$$

where $\Delta\boldsymbol{\theta}_I$ denotes the incremental rotational pseudovector.

In the case of folded structures, the folds between adjacent elements are modeled as rigid intersections. In intersections the drill rotations are supported by adjacent elements [23]. For that reason the incremental rotational pseudovector $\Delta\boldsymbol{\theta}_I$ can now be incorporated directly, so that three independent rotational degrees of freedom are applied. The associated director increment $\Delta\boldsymbol{t}_{eI}$ of a nodal unit director $\boldsymbol{t}_{eI}$ can be obtained for each adjacent element by

$$\Delta\boldsymbol{t}_{eI} = \Delta\boldsymbol{\theta}_I \times \boldsymbol{t}_{eI}^{(k)}. \tag{28}$$

In either case, the components of $\Delta\boldsymbol{t}$ are taken with respect to the global Cartesian coordinate system. The updated unit nodal director $\boldsymbol{t}_I^{(k+1)}$ and the updated orthogonal matrix $\boldsymbol{\Lambda}_I^{(k+1)}$ are given by

$$\boldsymbol{t}_I^{(k+1)} = \Delta\boldsymbol{\Lambda}_I\,\boldsymbol{t}_I^{(k)} \quad \text{and} \quad \boldsymbol{\Lambda}_I^{(k+1)} = \Delta\boldsymbol{\Lambda}_I\,\boldsymbol{\Lambda}_I^{(k)} \tag{29}$$

where $\Delta\boldsymbol{\Lambda}_I$ represents an orthogonal matrix associated with the finite rotational pseudovector $\Delta\boldsymbol{\theta}_I$ [24]

$$\Delta\boldsymbol{\Lambda}_I = \mathbf{1} + \frac{\sin\theta}{\theta}\,\widehat{\boldsymbol{\theta}} + \frac{1}{2}\left(\frac{\sin\theta/2}{\theta/2}\right)^2 \widehat{\boldsymbol{\theta}}^2 \tag{30}$$

where $\theta = |\Delta\boldsymbol{\theta}_I|$ and $\widehat{\boldsymbol{\theta}}$ denotes the skewsymmetric matrix associated with the axial vector $\Delta\boldsymbol{\theta}_I$, defined by the relation $\widehat{\boldsymbol{\theta}}\boldsymbol{a} = \Delta\boldsymbol{\vartheta}_I \times \boldsymbol{a}$ for any $\boldsymbol{a} \in \mathbb{R}^3$.

The update of the unit director field is obtained from the isoparametric interpolation of the incremental director field

$$\Delta\boldsymbol{t}(\xi, \eta) = \sum_{I=1}^{4} N^I(\xi, \eta)\,\Delta\boldsymbol{t}_I \tag{31}$$

via the following expressions, with $t = |\Delta\boldsymbol{t}|$

$$\boldsymbol{t}^{(k+1)} = \cos t\,\boldsymbol{t}^{(k)} + \frac{\sin t}{t}\,\Delta\boldsymbol{t} \tag{32}$$

$$\boldsymbol{t}_{,\alpha}^{(k+1)} = \cos t\,\boldsymbol{t}_{,\alpha}^{(k)} \tag{33}$$

$$+ \left(\frac{\sin t}{t}(\mathbf{1} - \boldsymbol{t}^{(k)} \otimes \Delta\boldsymbol{t}) + \frac{1}{t^2}\left[\cos t - \frac{\sin t}{t}\right]\Delta\boldsymbol{t} \otimes \Delta\boldsymbol{t}\right)\Delta\boldsymbol{t}_{,\alpha}. \tag{34}$$

REMARK 1. The usual kind of director interpolation applied to the degenerated concept

$$\boldsymbol{t}(\xi,\eta)=\sum_{I=1}^{4}N^{I}(\xi,\eta)\boldsymbol{t}_{I} \tag{35}$$

in general violates the inextensibility condition $|\boldsymbol{t}|=1$ within the element domain. As noted in [25], due to this defect shell elements based on the plane stress assumption turn out to be too flexible, in particular for a coarse mesh and low order elements. In the present work the shortcomings of the analogous interpolation of the extensible director field $\boldsymbol{d}(\xi,\eta)$ are far more significant, especially when large curvatures occur. This is due to the fact, that artificial thickness strains are computed via $(14)_3$ which, in combination with three dimensional material models lead to pathological behaviour. The employed interpolation (31) in conjunction with the multiplicative decomposition (3) leads on the one hand to a more elaborate formulation but on the other hand circumvents the spurious thickness strains.

In the present work we employ the following direct interpolation of the thickness stretch field

$$\lambda(\xi,\eta)=\sum_{I=1}^{4}N^{I}(\xi,\eta)\lambda_{I} \tag{36}$$

such that the actual shell thickness yields $h^{(k)}=\lambda^{(k)}h_0$. We further make use of the simple additive update formula

$$\lambda^{(k+1)}=\lambda^{(k)}+\Delta\lambda \tag{37}$$

which accounts for deformation induced thickness change, with initial thickness stretch $\lambda^{(0)}=1$ in the reference configuration. Thus, the updated discrete extensible director field preserves the structure of the multiplicative decomposition (3)

$$\boldsymbol{d}^{(k+1)}=\lambda^{(k+1)}\boldsymbol{t}^{(k+1)} \tag{38}$$

REMARK 2. In the extensible shell theory of Simo et al. [15] logarithmic strain components have been defined so that the thickness stretch does not appear any more in the weak form. Therefore, in [15] the logarithmic stretch has been interpolated. Since the present formulation is based on the covariant Green–Lagrangian strains, see (15), the thickness stretch appears directly in the corresponding weak form. This motivates the direct interpolation of the thickness stretch (36).

4.2. *Interpolation of the enhanced strains*

The introduced extensible director field (3) allows for constant thickness strains $(16)_3$ corresponding to a linear displacement field over the shell thickness. However, as demonstrated in [26] for hierarchic shell models within the context of linear 3D-elasticity at least a quadratic displacement field and therefore a linear distribution of the thickness strains over the shell thickness is required. According to [26], a shell model characterized by displacement components which are linear functions in transverse direction converges to a different solution compared to the Reissner–Mindlin shell model in the asymptotic case of vanishing thickness if Poisson's ratio is not equal to zero.

In the present work, one possible remedy would be to use more costly shell kinematics which allow for a quadratic displacement field over the shell thickness. On the other side this would lead to a higher number of nodal degrees of freedom and to more complicated expressions, especially for the geometrical part of the Hessian matrix.

We follow another solution strategy which relies on the enhanced assumed strain method and has been proposed recently by Büchter et al. [14]. Therefore, linearly varying thickness strains over the thickness are introduced by the following expansion for the enhanced thickness strains (in the present work slightly modified by the factor $\sqrt{G_0/G}$)

$$\tilde{E}_{33}(\xi,\eta,\xi^3)=\frac{\sqrt{G_0}}{\sqrt{G}}\xi^3\boldsymbol{g}^{\mathrm{T}}\boldsymbol{\alpha}_e^{\mathrm{II}}$$
$$\text{with}\quad \boldsymbol{g}^{\mathrm{T}}=[1,\ \xi,\ \eta,\ \xi\eta],\qquad \boldsymbol{\alpha}_e^{\mathrm{II}}=[\alpha_1,\ \alpha_2,\ \alpha_3,\ \alpha_4]_e^{\mathrm{T}} \tag{39}$$

where $\boldsymbol{\alpha}_e^{\mathrm{II}}$ contains four local element strain parameters associated with the interpolation vector $\boldsymbol{g}$ which defines the interpolation in the isoparametric domain. The subscript 0 refers throughout to a quantity evaluated at the center of the element. Accordingly, the compatible constant thickness strains are enriched by the enhanced linear term when required by bending deformation. The following orthogonality condition holds for at least constant stress components S^{33}

$$\int_{\mathcal{B}_0^e} S^{33}\tilde{E}_{33}\,\mathrm{d}V=\int_{\square}\left[\int_{-h_0/2}^{h_0/2} S^{33}\xi^3\,\mathrm{d}\xi^3\right]\boldsymbol{g}^{\mathrm{T}}\,\mathrm{d}\xi\,\mathrm{d}\eta\,\boldsymbol{\alpha}_e^{\mathrm{II}}=0 \tag{40}$$

where $\square$ denotes the biunit square in $\mathbb{R}^2$.

We further enhance the compatible tangential strains $(16)_{\mathrm{I}}$ to reach an improved membrane behaviour of the bilinear shell element, especially for in-plane bending dominated cases. We define the following expansion of the enhanced tangential strains $\tilde{E}_{\alpha\beta}$

$$\tilde{E}_{\alpha\beta}\boldsymbol{G}^{\alpha}\otimes\boldsymbol{G}^{\beta}=\frac{\sqrt{G_0}}{\sqrt{G}}\tilde{\Xi}_{\gamma\delta}\boldsymbol{G}_0^{\gamma}\otimes\boldsymbol{G}_0^{\delta}. \tag{41}$$

Accordingly, the interpolated components $\tilde{\Xi}_{\alpha\beta}$ are referred to the contravariant base vectors $\boldsymbol{G}_0^{\alpha}$ at the center of the element.

REMARK 3. According to Simo and Rifai [18] the interpolated strains $\tilde{\boldsymbol{\Xi}}$ in isoparametric space are convected to the reference configuration via the transformation

$$\tilde{\boldsymbol{E}}=\frac{\det[\boldsymbol{J}_{\alpha}]}{\det[\boldsymbol{J}]}\boldsymbol{J}_0^{-\mathrm{T}}\tilde{\boldsymbol{\Xi}}\boldsymbol{J}_0^{-1}. \tag{42}$$

The reference Jacobian $\boldsymbol{J}=\mathrm{Grad}_{\boldsymbol{\xi}}[\boldsymbol{X}]$ is evaluated in the center of the element, i.e. $\boldsymbol{J}_0=\boldsymbol{J}(\boldsymbol{\xi}=\boldsymbol{0})$, so that patch test requirements are satisfied. In [18] the strains are expressed in the global Cartesian frame. Alternatively, we apply the expression $\boldsymbol{J}_0^{-1}=\boldsymbol{e}_i\otimes\boldsymbol{G}_0^i$ in order to obtain the suggested expansion (41) which accounts for the present covariant strain formulation in a natural way.

Furthermore, we assume interpolations, discontinuous over element boundaries, of the form

$$\begin{bmatrix}\tilde{\Xi}_{11}\\ \tilde{\Xi}_{22}\\ 2\tilde{\Xi}_{12}\end{bmatrix}=\begin{bmatrix}\xi & 0 & 0 & 0 & 0\\ 0 & \eta & 0 & 0 & 0\\ 0 & 0 & \xi & \eta & \xi\eta\end{bmatrix}\begin{bmatrix}\alpha_5\\ \alpha_6\\ \alpha_7\\ \alpha_8\\ \alpha_9\end{bmatrix} \tag{43}$$

$$\tilde{\boldsymbol{\Xi}}=\boldsymbol{\Gamma}\boldsymbol{\alpha}_e^{m}$$

The matrix $\boldsymbol{\Gamma}$ contains the interpolation functions for the enhanced tangential strain field $\tilde{\Xi}_{\alpha\beta}$ in isoparametric space. The form of the interpolation field is motivated by examining the polynomial expansion of the compatible strains in isoparametric space of a four-node membrane element. For the infinitesimal theory this procedure has been investigated by Andelfinger and Ramm [27]. In the present case the non-linear components of the Green–Lagrangian strain tensor in isoparametric space read

$$E_{\alpha\beta}^{C}=\frac{1}{2}\left[\frac{\partial\boldsymbol{u}}{\partial\xi^{\beta}}\cdot\boldsymbol{G}_{\alpha}+\frac{\partial\boldsymbol{u}}{\partial\xi^{\alpha}}\cdot\boldsymbol{G}_{\beta}+\frac{\partial\boldsymbol{u}}{\partial\xi^{\alpha}}\cdot\frac{\partial\boldsymbol{u}}{\partial\xi^{\beta}}\right] \tag{44}$$

such that the compatible strain field of the bilinear membrane element is of the form

$$E^C_{\alpha\beta} \in \operatorname{span}\begin{bmatrix} 1 & 0 & 0 & \eta & 0 & 0 & 0 & \eta^2 & 0 & 0 \\ 0 & 1 & 0 & 0 & \xi & 0 & 0 & 0 & \xi^2 & 0 \\ 0 & 0 & 1 & 0 & 0 & \xi & \eta & 0 & 0 & \xi\eta \end{bmatrix} . \tag{45}$$

The five-parameter interpolation (43) is chosen in order to decouple and enhance the compatible strains. The orthogonality condition for at least constant stresses holds for

$$\int \boldsymbol{\Gamma}\, \mathrm{d}\xi\, \mathrm{d}\eta\, \mathrm{d}\xi^3 = 0 . \tag{46}$$

In order to obtain the assumed tangential strain field $E_{\alpha\beta} = E^C_{\alpha\beta} + \tilde{E}_{\alpha\beta}$ we apply the transformation

$$\tilde{E}_{\gamma\delta} = \frac{\sqrt{G_0}}{\sqrt{G}} (\boldsymbol{G}_\gamma \cdot \boldsymbol{G}^\alpha_0)\tilde{\Xi}_{\alpha\beta}(\boldsymbol{G}^\beta_0 \cdot \boldsymbol{G}_\delta) . \tag{47}$$

The required contravariant base vectors $\boldsymbol{G}^\alpha_0$ at the center of the element can be calculated via

$$\boldsymbol{G}^\alpha_0 = G^{\alpha\beta}_0 \boldsymbol{G}_{0\beta} , \qquad \boldsymbol{G}_{0\alpha} = \left[\frac{\partial \boldsymbol{\Phi}}{\partial \xi^\alpha}\right]_{\xi^1 \xi^2 = 0}$$

$$\text{with} \quad [G^{\alpha\beta}_0] = [G_{0\alpha\beta}]^{-1} \quad \text{and} \quad G_{0\alpha\beta} = \boldsymbol{G}_{0\alpha} \cdot \boldsymbol{G}_{0\beta} \tag{48}$$

The transformation (47) can be expressed in the usual finite element vector notation as

$$\begin{bmatrix} \tilde{E}_{11} \\ \tilde{E}_{22} \\ 2\tilde{E}_{12} \end{bmatrix} = \frac{\sqrt{G_0}}{\sqrt{G}} \begin{bmatrix} a^2_{11} & a^2_{12} & a_{11}a_{12} \\ a^2_{21} & a^2_{22} & a_{21}a_{22} \\ 2a_{11}a_{21} & 2a_{12}a_{22} & a_{11}a_{22} + a_{12}a_{21} \end{bmatrix} \begin{bmatrix} \tilde{\Xi}_{11} \\ \tilde{\Xi}_{22} \\ 2\tilde{\Xi}_{12} \end{bmatrix} \tag{49}$$

$$\tilde{\boldsymbol{E}}_m = \boldsymbol{A}\tilde{\boldsymbol{\Xi}} = \tilde{\boldsymbol{G}}\boldsymbol{\alpha}^m_e , \qquad \tilde{\boldsymbol{G}} = \boldsymbol{A}\boldsymbol{\Gamma} \tag{50}$$

where $a_{\alpha\beta} = \boldsymbol{G}_\alpha \cdot \boldsymbol{G}^\beta_0$.

For the subsequent finite element formulation it proves convenient to use the following matrix notation for the strain components

$$\boldsymbol{E} = [E_{11}, E_{22}, 2E_{12}, E_{33}, 2E_{13}, 2E_{23}]^{\mathrm{T}} \tag{51}$$

The interpolation for the enhanced strains can now be written

$$\tilde{\boldsymbol{E}} = \boldsymbol{G}\boldsymbol{\alpha}_e \quad \text{where} \quad \boldsymbol{G} = \begin{bmatrix} \boldsymbol{0}_{3\times 4} & \tilde{\boldsymbol{G}}_{3\times 5} \\ \dfrac{\sqrt{G_0}}{\sqrt{G}} \xi^3 \boldsymbol{g}^{\mathrm{T}}_{1\times 4} & \boldsymbol{0}_{1\times 5} \\ \boldsymbol{0}_{2\times 4} & \boldsymbol{0}_{2\times 5} \end{bmatrix} \tag{52}$$

with $\boldsymbol{\alpha}_e = [\boldsymbol{\alpha}^d_e, \boldsymbol{\alpha}^m_e]^{\mathrm{T}}$ the vector of the local strain parameters.

4.3. Treatment of transverse shear strains

In order to avoid shear locking of the displacement formulation, we employ the assumed natural strain method, as applied to the four-node shell element in [28]. Accordingly, the constant-linear interpolations for the assumed transverse shear strains are based on the compatible transverse shear strains (16)$_2$ collocated at the midpoints $Q = A, B, C, D$ of the element boundaries.

$$\begin{bmatrix} 2\tilde{E}_{13} \\ 2\tilde{E}_{23} \end{bmatrix} = \begin{bmatrix} (1-\eta)E^B_{13} + (1+\eta)E^D_{13} \\ (1-\xi)E^A_{23} + (1+\xi)E^C_{23} \end{bmatrix} \tag{53}$$

These interpolations eliminate the spurious modes of the compatible transverse shear strains and allow for pure bending deformations without parasitic transverse shear strains.

4.4. Discrete weak form

Due to the orthogonality condition between discontinuous stress and enhanced strain interpolations, the Second Piola–Kirchhoff stress field is effectively eliminated from the variational equations (21). The mixed finite element approximation of the remaining two-field variational equations with generalized element displacement vectors $\boldsymbol{v}_e = [\boldsymbol{\varphi},\ \boldsymbol{t},\ \lambda]_e^{\mathrm{T}}$ and $\delta\boldsymbol{v}_e = [\delta\boldsymbol{\varphi},\ \delta\boldsymbol{t},\ \delta\lambda]_e^{\mathrm{T}}$ reads

$$\begin{aligned}
&\sum_{e=1}^{n_{\mathrm{elem}}} \left[\int_{\mathcal{B}_0^e} \delta\boldsymbol{E}^C(\boldsymbol{v}_e) \cdot \frac{\partial \hat{W}_{0S}}{\partial \boldsymbol{E}}(\boldsymbol{v}_e, \boldsymbol{\alpha}_e)\, \mathrm{d}V - G_e^{\mathrm{ext}}(\delta\boldsymbol{v}_e) \right] = 0 \\
&\int_{\mathcal{B}_0^e} \delta\tilde{\boldsymbol{E}}(\boldsymbol{\alpha}_e) \cdot \frac{\partial \hat{W}_{0S}}{\partial \boldsymbol{E}}(\boldsymbol{v}_e, \boldsymbol{\alpha}_e)\, \mathrm{d}V = 0 \quad \text{for } e = 1, 2, \ldots, n_{\mathrm{elem}}.
\end{aligned} \tag{54}$$

The linearization of the compatible strain measures (16) at $\boldsymbol{v}_e$ can be obtained via the discrete operator matrix $\boldsymbol{B}_I$, presented in Appendix A.1, from the variation of the nodal kinematic variables $\delta\boldsymbol{v}_I = [\delta\boldsymbol{\varphi}_I,\ \delta\boldsymbol{t}_I,\ \delta\lambda_I]^{\mathrm{T}}$

$$\delta\boldsymbol{E}^C(\boldsymbol{v}_e) = \sum_{I=1}^{4} \boldsymbol{B}_I(\boldsymbol{v}_e)\, \delta\boldsymbol{v}_I \tag{55}$$

In addition to alleviate the notation we define

$$\hat{\boldsymbol{S}}(\boldsymbol{v}_e, \boldsymbol{\alpha}_e) = \frac{\partial \hat{W}_{0S}}{\partial \boldsymbol{E}} \tag{56}$$

with corresponding ordering of the components in column-matrix form

$$\hat{\boldsymbol{S}} = [\hat{S}^{11}, \hat{S}^{22}, \hat{S}^{12}, \hat{S}^{33}, \hat{S}^{13}, \hat{S}^{23}]^{\mathrm{T}} \tag{57}$$

and we obtain the discrete weak form

$$\begin{aligned}
&\sum_{e=1}^{n_{\mathrm{elem}}} \sum_{I=1}^{4} \delta\boldsymbol{v}_{eI}^{\mathrm{T}} \left[\int_{\mathcal{B}_0^e} \boldsymbol{B}_I^{\mathrm{T}}(\boldsymbol{v}_e) \hat{\boldsymbol{S}}(\boldsymbol{v}_e, \boldsymbol{\alpha}_e)\, \mathrm{d}V - \boldsymbol{f}_{eI}^{\mathrm{ext}} \right] = 0 \\
&\delta\boldsymbol{\alpha}_e^{\mathrm{T}} \int_{\mathcal{B}_0^e} \boldsymbol{G}^{\mathrm{T}} \hat{\boldsymbol{S}}(\boldsymbol{v}_e, \boldsymbol{\alpha}_e)\, \mathrm{d}V = 0 \quad \text{for } e = 1, 2, \ldots, n_{\mathrm{elem}}.
\end{aligned} \tag{58}$$

The system of non-linear equations (58) can be solved for the generalized nodal displacements $\boldsymbol{v}$ and the local element strain parameters $\boldsymbol{\alpha}_e$ by an iterative solution procedure. Newtons method requires the consistent linearization of the discrete weak form (58). Since the enhanced strains are chosen discontinuously across the element boundaries the elimination of the internal degrees of freedom $\boldsymbol{\alpha}_e$ at the element level is possible. Accordingly, after assembly, we obtain the generalized displacement problem

$$\boldsymbol{K}_t^{(k)} \Delta\boldsymbol{v} = \boldsymbol{R}^{(k)} \tag{59}$$

with

$$\begin{aligned}
\boldsymbol{K}_t^{(k)} &= \mathop{\mathbf{A}}_{e=1}^{n_{\mathrm{elem}}} (\boldsymbol{K}_e^{(k)} - \boldsymbol{\Gamma}_e^{(k)\mathrm{T}} \boldsymbol{H}_e^{(k)-1} \boldsymbol{\Gamma}_e^{(k)}) \\
\boldsymbol{R}^{(k)} &= \mathop{\mathbf{A}}_{e=1}^{n_{\mathrm{elem}}} (\boldsymbol{\Gamma}_e^{(k)T} \boldsymbol{H}_e^{(k)-1} \boldsymbol{h}_e^{(k)} - \boldsymbol{f}_e^{\mathrm{int}(k)} + \boldsymbol{f}_e^{\mathrm{ext}})
\end{aligned} \tag{60}$$

where

$$\boldsymbol{K}_e^{(k)} = \sum_{I=1}^{4} \sum_{J=1}^{4} \int_{\mathcal{B}_0^e} [\boldsymbol{B}_I^{\mathrm{T}}(\boldsymbol{v}_e^{(k)}) \hat{\boldsymbol{C}}^{(k)} \boldsymbol{B}_J(\boldsymbol{v}_e^{(k)}) + \boldsymbol{G}_{IJ}(\boldsymbol{v}_e^{(k)}, \boldsymbol{\alpha}_e^{(k)})]\, \mathrm{d}V \tag{61}$$

defines the contribution to the tangent stiffness matrix $(60)_1$ similar to pure displacement formulations.

The matrix $\boldsymbol{G}_{IJ}$ represents the geometric part and is included in Appendix A.2. Furthermore

$$\widehat{\boldsymbol{C}}^{(k)} = \frac{\partial^2 \hat{W}_{0v}}{\partial \boldsymbol{E}\, \partial \boldsymbol{E}} (\boldsymbol{v}_e^{(k)}, \boldsymbol{\alpha}_e^{(k)}) \tag{62}$$

denotes the matrix of tangent elastic moduli associated with $(\boldsymbol{v}_e^{(k)}, \boldsymbol{\alpha}_e^{(k)})$. Further, we obtain

$$\boldsymbol{I}_e^{(k)} = \sum_{J=1}^{4} \int_{\mathcal{B}_0^e} \boldsymbol{G}^{\mathrm{T}} \widehat{\boldsymbol{C}}^{(k)} \boldsymbol{B}_J(\boldsymbol{v}_e^{(k)})\, \mathrm{d}V \qquad \boldsymbol{H}_e^{(k)} = \int_{\mathcal{B}_0^e} \boldsymbol{G}^{\mathrm{T}} \widehat{\boldsymbol{C}}^{(k)} \boldsymbol{G}\, \mathrm{d}V \tag{63}$$

$$\boldsymbol{f}_e^{\mathrm{int}(k)} = \sum_{I=1}^{4} \int_{\mathcal{B}_0^e} \boldsymbol{B}_I^{\mathrm{T}}(\boldsymbol{v}_e^{(k)}) \widehat{\boldsymbol{S}}(\boldsymbol{v}_e^{(k)}, \boldsymbol{\alpha}_e^{(k)})\, \mathrm{d}V \qquad \boldsymbol{h}_e^{(k)} = \int_{\mathcal{B}_0^e} \boldsymbol{G}^{\mathrm{T}} \widehat{\boldsymbol{S}}(\boldsymbol{v}_e^{(k)}, \boldsymbol{\alpha}_e^{(k)})\, \mathrm{d}V \tag{64}$$

and $\boldsymbol{f}_e^{\mathrm{ext}}$ is the vector of the external forces following from (20). After solution of the associated linear system of equations the enhanced strain parameters and the configuration are updated by

$$\begin{aligned} &\boldsymbol{\alpha}_e^{(k+1)} = \boldsymbol{\alpha}_e^{(k)} - \boldsymbol{H}_e^{(k)-1}(\boldsymbol{h}_e^{(k)} + \boldsymbol{I}_e^{(k)} \Delta \boldsymbol{v})\,, \\ &\boldsymbol{v}^{(k)} \to \boldsymbol{v}^{(k+1)} \quad \text{with} \quad \Delta \boldsymbol{v} \end{aligned} \tag{65}$$

where the configuration update is outlined in Section 4.1.

REMARK 4. In comparison to the non-linear enhanced assumed strain formulation of Simo and Armero [19] in the present Lagrangian formulation only the common geometrical part $\boldsymbol{G}_{IJ}$ of the tangent stiffness matrix appears. Thus the geometrical part $\boldsymbol{G}_{IJ}$ is identical to displacement based elements. The enhancement of the displacement gradient in [19] leads to further geometrical contributions in the linearized weak form.

5. Numerical examples

The element scheme has been implemented in an enhanced version of the program FEAP documented in [29]. In this section several linear and non-linear examples show that in the thin-shell limit plane stress response is recovered. Furthermore, examples with rubberlike material show the ability of the element to model large strains. We refer to the Appendix A.3, where the constitutive tensor and the stress–strain relation are given in detail.

5.1. In-plane bending of a beam; mesh distortion

This problem has been investigated previously by Simo et al. [4] to show the superior performance of their mixed finite shell element formulation for the membrane field based on the Hellinger–Reissner functional. A cantilever beam subjected to an end load is discretized with 10 finite elements. The first mesh contains regular elements, whereas the second is generated with highly distorted elements, see Fig. 1. The material properties used for this problem are $E = 10^7$ and $\nu = 0.3$, the beam length is $L = 1.0$ and the width and thickness are $w = h_0 = 0.1$. A load deflection curve for both meshes is shown in Fig. 1. The present shell element based on the enhanced assumed strain method shows the same accurate results and insensitivity to mesh distortion as reported in [4].

5.2. Thin beam bending

This simple problem shows on the one hand that the plane stress solution is recovered in the thin-shell limit and on the other hand the significance of the enhanced thickness strains $\tilde{E}_{33}$.

A beam of length $L = 10$ and width $b = 1$ is clamped on one end and subjected to two point loads acting on the mid-surface of the free end, see Fig. 2. Three different values for the beam thickness $h_0 = 1$, 0.1 and 0.01 lead to Length to thickness ratios of 10, 100 and 1000.

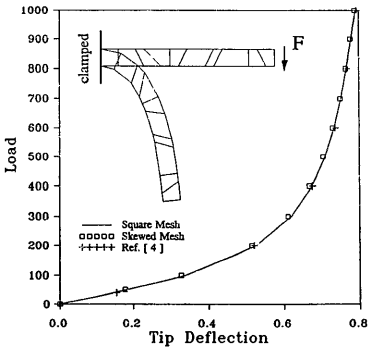

Fig. 1. In-plane beam bending problem, initial and deformed mesh configuration of the arbitrarily distorted mesh and load-deflection curves.

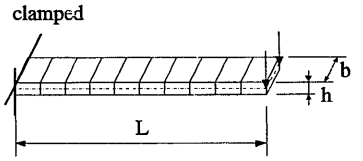

Fig. 2. Problem definition and mesh discretization of the thin beam bending problem.

Ten elements are used to model this problem, with material properties $E = 10^7$ and $\nu = 0.4$. In the non-linear calculations the applied load is increased in five load steps up to $F = 5 \times 10^4 h_0^3$. The results are compared with a stress resultant shell formulation based on the plane stress assumption (see [30]).

The obtained results for the tip deflection under point load are listed in Tables 1 and 2. It can be seen, that the present element yields the plane stress response in the thin-shell limit. Furthermore, the importance of the enhanced thickness strains (39) is demonstrated both for the linear and non-linear case.

5.3. *Shearing of a twisted ribbon*

This linear problem, a shell twisted 90°, is an excellent test to assess the effect of warping on the performance of the shell element (see [31]). A shell of length $l = 12$, width $w = 1.1$, thickness $h_0 = 0.32$, and material properties $E = 2.9 \times 10^7$, $\nu = 0.22$ is clamped and subjected to a shear load in thickness direction $F = 1$, see Fig. 3. The displacements in load direction are reported for a sequence of finite element meshes in Table 3. They are normalized with respect to the theoretical solution $u = 1.754 \times 10^{-3}$ [31]. The significance of the enhanced strains $\bar{E}_{33}$ and $\bar{E}_{\alpha\beta}$ is evident, especially for coarse meshes.

Table 1
Thin beam bending, $h_0 = 0.01$, $F = 1$, linear calculation

Plane stress shell element	Present shell element	
	with $\bar{E}_{33}$	without $\bar{E}_{33}$
3.924	3.924	3.173

Table 2
Thin beam bending, $F = 5 \times 10^4 h_0^3$, non-linear calculation

L/h Ratio	10		100		1000	
Displacement	vertical	horizontal	vertical	horizontal	vertical	horizontal
Plane stress	7.498	4.360	7.411	4.314	7.410	4.314
Present with $\bar{E}_{33}$	7.513	4.388	7.412	4.316	7.411	4.315
Without $\bar{E}_{33}$	7.100	3.830	6.998	3.762	6.998	3.761

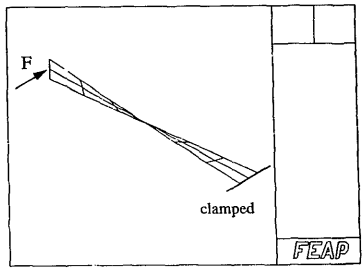

Fig. 3. Shearing of a twisted ribbon. Problem definition and mesh discretization.

Table 3
Shearing of a twisted ribbon, normalized displacements in load direction

Mesh	1 × 6	2 × 12	2 × 24	4 × 48
With $\hat{E}_{33}$	0.788	0.914	0.970	0.990
With $\hat{E}_{33}$ and $\hat{E}_{\alpha\beta}$	0.934	0.979	0.993	0.996
Without $\hat{E}_{33}, \hat{E}_{\alpha\beta}$	0.726	0.879	0.934	0.954

5.4. *Pinched hemisphere with 18° hole*

A hemispherical shell with an 18° hole at the top is loaded at the free edge with two inward and two outward forces 90° apart. Symmetry conditions are used on this problem and only one quarter of the shell is modeled. The material properties are $E = 6.825 \times 10^7$ and $\nu = 0.3$, the radius is $R = 10$ and the thickness is $h_0 = 0.04$.

The results obtained for the linear case are listed in Table 4. The values for the displacements under the loads are compared to those reported in [15] for a stress resultant mixed shell formulation. The obtained results for the non-linear case are plotted in Fig. 5 and compared to the plane stress resultant shell element in [4]. It can be seen, that the plane stress response in the thin-shell limit is recovered by the present shell formulation. Fig. 4 contains a plot of the initial and deformed mesh configurations.

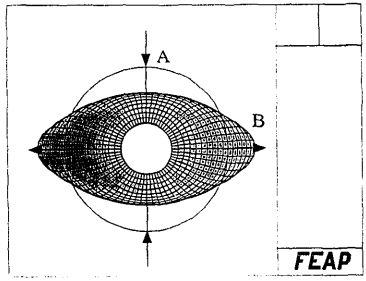

Fig. 4. Pinched hemisphere with 18° hole. Outline of the initial configuration and deformed mesh configuration of the non-linear calculation. $F = 100$.

Table 4
Pinched hemisphere, $h_0/R = 4 \cdot 10^{-3}$, $F = 1$, linear calculation

Elements	4×4	8×8	16×16
Ref. [15]	0.092530	0.092697	0.092990
Present with $\hat{E}_{33}$	0.091577	0.092262	0.092745
Without $\hat{E}_{33}$	0.090320	0.091858	0.092426
With $\hat{E}_{33}$ and $\hat{E}_{\alpha\beta}$	0.091596	0.092472	0.092990

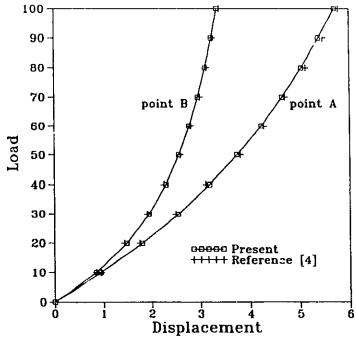

Fig. 5. Pinched hemisphere, $h_0/R = 4 \cdot 10^{-3}$, load-deflection curves of the non-linear calculation.

5.5. Channel-section beam

A channel-section beam clamped at one end and subjected to a tip force at the free end has been investigated previously in [32]. The data describing the problem are: length $L = 36$, width $a = 2$, height $b = 6$, thickness $h_0 = 0.05$, see Fig. 6, elasticity data $E = 1 \times 10^7$, $\nu = 0.333$. We model the intersections

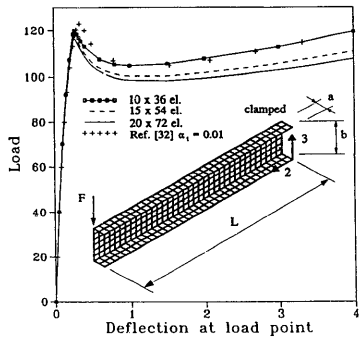

Fig. 6. Channel-section beam, problem description and load-deflection curves of the non-linear calculation.

of the folded plate structure as rigid intersections with 3 rotational degrees of freedom as described in section 4.1. At the remaining smooth parts the drilling degree of freedom is eliminated and 2 rotational degrees of freedom are used.

Table 5 summarizes the computed deflection w in load direction under an applied load $F = 1$, for the linear calculation. A sequence of $n \times m$ meshes is considered with n elements along the width/height and m elements along the length direction.

The load-deflection results for the non-linear calculation are plotted in Fig. 6. They are compared to solutions given in [32], which depend on a 'torsional coefficient' α_t. Fig. 7 contains a plot of the initial and deformed configuration.

5.6. *Cooks membrane problem*

This finite deformation elasticity problem has been considered by Simo and Armero [19] to show the superior behaviour of of their Q1/E4 element, where in the geometrically non-linear regime the material displacement gradient has been enhanced.

Using the present shell element, the plane strain condition is modeled by constraining the thickness extensibility as a boundary condition ($\Delta\lambda = 0$). The material properties for the compressible Neo-Hookean material model (see Appendix A.3) are $K = 40.0942 \cdot 10^4$ and $\mu = 80.1938$, so that quasi-incompressible response is effectively obtained.

The problem has been discretized by 2×2, 4×4, 8×8, 16×16 and 32×32 finite element meshes. In Fig. 8 the vertical displacement of the top edge node is plotted versus the number of elements per side. It can be seen that the present formulation, employing the enhanced Green–Lagrangian strain tensor, leads to the same accurate results as reported in [19].

We remark further, that the pure displacement formulation (obtained in the present formulation by merely dropping the enhanced tangential strains $\tilde{E}_{\alpha\beta}$) exhibits severe locking in the incompressible limit.

Table 5
Channel-section beam, linear calculation

Elements	5×18	10×36	15×54	20×72
Displacement $w \times 10^3$	1.0186	1.0998	1.1190	1.1293

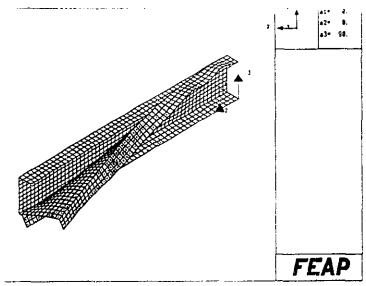

Fig. 7. Initial and deformed mesh configuration (15×54 elements) of the Channel-section beam.

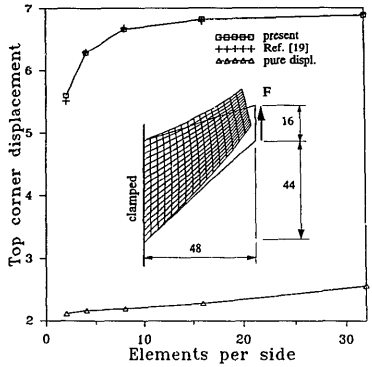

Fig. 8. Description and results of Cooks membrane problem. Final deformed 16 × 16 mesh configuration for quasi-incompressible finite deformation elasticity. The top corner displacement is plotted for a sequence of refined meshes, $F = 100$.

5.7. *Bending and inflation of a circular plate*

This finite deformation problem has been previously investigated by the authors in [9, 10]. A circular plate with radius $r = 7.5$ and thickness $h_0 = 0.5$ is simply supported at the circumference and subjected to uniform pressure acting perpendicular to the current configuration. The plate is made of an incompressible hyperelastic material described by the Mooney–Rivlin model (see Appendix A.3) with material constants $c_1 = 80$ and $c_2 = 20$. We enforce the incompressibility constraint by means of the augmented Lagrangian technique (see e.g. [34] and references therein). The deformation dependent pressure leads to an additional (non-symmetric) contribution to the tangential stiffness matrix $(60)_1$ (see e.g. [33]).

Because of the symmetry of the problem, only one quarter of the plate has been modeled with 27 and 108 elements, respectively. In Fig. 9 the applied value of the pressure is plotted versus the deflection of the plate center. The computed results, obtained with three Gauss integration points through the thickness, are compared to calculations using the membrane element presented in [33] and to the shell element of [23], respectively. Both formulations satisfy incompressibility in an exact manner using the plane stress condition. It can be seen that the results fit very well. Fig. 10 depicts a sequence of deformed configurations for increasing pressure loads.

5.8. *Stretching of a rubber sheet with a hole*

The last example is concerned with the stretching of a square sheet with a circular hole. This problem has been analyzed previously by Parisch [10]. As in the latter example incompressible material response is governed by the Mooney–Rivlin model (see Appendix A.3) with material constants $c_1 = 25$ and $c_2 = 7$. The length of the square is $2L = 20$, the radius of the circle is $R = 3$, and the thickness is $h_0 = 0.1$. Because of the symmetry of the problem, only one quarter of the specimen has been modeled with 200 elements. Fig. 11 depicts the outline of the initial geometry and the corresponding deformed mesh configuration for a edge displacement of $u = 10$.

Our calculations base on the arc-length-method with displacement control. At a load level of $F = 1.78$ we compute a bifurcation point which is due to a local instability of the sheet around the hole. A switch to the secondary path is possible by a perturbation of the primary solution with the first eigenvector. The secondary solution path is characterized by an out-of-plane deflection w. To catch this effect the

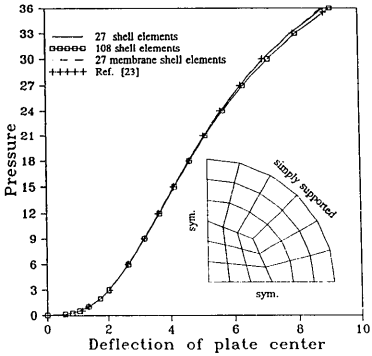

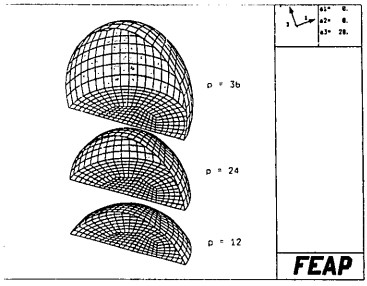

Fig. 9. Bending and inflation of a circular plate. Discretized quarter of the plate (27 elements) and plot of pressure versus deflection at plate center.

Fig. 10. Bending and inflation of a circular plate. Sequence of deformed configurations (mesh consists of 108 elements).

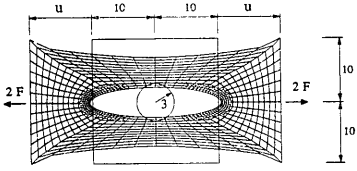

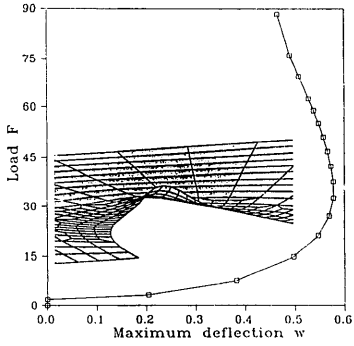

Fig. 11. Stretching of a rubber sheet with a hole. Description of the initial system and corresponding deformed mesh configuration for an edge displacement of $u = 10$.

Fig. 12. Stretching of a rubber sheet with a hole. Plot of maximum out-of-plane deflections obtained in the post-buckling analysis. Detailed view of the deformed mesh ($u = 3$).

mesh within the buckling domain is locally refined. Fig. 12 shows the maximum out-of-plane deflection values for different load levels, obtained in the post-buckling analysis. Furthermore a detailed view of the deformed mesh for a displacement level of $u = 3$ is shown. In Fig. 13 the stretching force F of the computed quarter is plotted against the displacement u. A comparing calculation with the membrane element developed in [33] shows that the local buckling state has no significant influence on the global deformation.

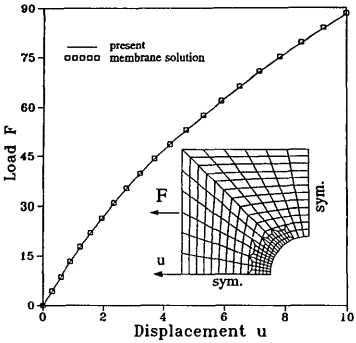

Fig. 13. Stretching of a rubber sheet with a hole. Applied load F versus displacement u.

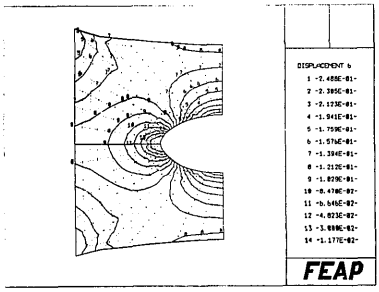

Fig. 14. Stretching of a rubber sheet with a hole. Contour values of the accumulated thickness stretch increments $\Delta\lambda$ ('DISPLACEMENT 6') for $u = 3$.

Fig. 14 contains a plot of contour values of accumulated thickness stretch increments $\Delta\lambda$ for a displacement level of $u = 3$. The corresponding thickness change Δh can be computed via $\Delta h = h_0 \cdot \Delta\lambda$. For this displacement level the maximum thickness change amounts to 24.88 %. The actual thickness h follows from $h = (1 + \Delta\lambda) \cdot h_0$.

6. Conclusions

In this paper a non-linear finite shell element formulation accounting for large elastic deformations is presented. The essential feature of our formulation is an interface to arbitrary three-dimensional material laws. The theory accounts for all stress and strain components of the three-dimensional constitutive equations. This is achieved using extensible director kinematics where the thickness stretch is an independent variable. Thus, the developed theory incorporates large rotations and large strains and applies to a wide class of non-linear hyperelastic constitutive equations. The Lagrangian formulation is based on a three-field variational principle parametrized with displacements, enhanced Green–Lagrangian strains and Second Piola–Kirchhoff stresses as independent variables. The resulting quadrilateral shell element is developed within the degenerated concept. Thus, numerical integration through the thickness circumvents usual shell approximations for the constitutive equations. The element is characterized by coarse mesh accuracy and distortion insensitivity compared with bilinear displacement approaches. Several linear and non-linear examples show that in the asymptotic case of vanishing thickness plane stress response is recovered. Further examples with rubberlike material show the ability of the element to model large strains.

Acknowledgement

We thank P. Steinmann and W. Wagner for helpful comments and many discussions.

Appendix A

A.1. Linearized strain-nodal configuration operator

The linearized compatible tangential strains $(16)_1$ and thickness strains $(16)_3$ are related to the kinematic variables of node I by the following part of the discrete operator matrix (55) (with $(\cdot)_{,1} = \partial(\cdot)/\partial\xi$ and $(\cdot)_{,2} = \partial(\cdot)/\partial\eta$)

$$\begin{bmatrix} \delta E_{11} \\ \delta E_{22} \\ 2\delta E_{12} \\ \delta E_{33} \end{bmatrix} = \sum_{I=1}^{4} \begin{bmatrix} N^I_{,1}\boldsymbol{g}_1^{\mathrm{T}} & \xi^3 l^I_1 \boldsymbol{g}_1^{\mathrm{T}} & \xi^3 \boldsymbol{g}_1^{\mathrm{T}} \boldsymbol{m}^I_1 \\ N^I_{,2}\boldsymbol{g}_2^{\mathrm{T}} & \xi^3 l^I_2 \boldsymbol{g}_2^{\mathrm{T}} & \xi^3 \boldsymbol{g}_2^{\mathrm{T}} \boldsymbol{m}^I_2 \\ N^I_{,1}\boldsymbol{g}_2^{\mathrm{T}} + N^I_{,2}\boldsymbol{g}_1^{\mathrm{T}} & \xi^3[l^I_1 \boldsymbol{g}_2^{\mathrm{T}} + l^I_2 \boldsymbol{g}_1^{\mathrm{T}}] & \xi^3[\boldsymbol{g}_2^{\mathrm{T}} \boldsymbol{m}^I_1 + \boldsymbol{g}_1^{\mathrm{T}} \boldsymbol{m}^I_2] \\ \boldsymbol{0}_{1\times 3} & \boldsymbol{0}_{1\times 3} & \lambda N^I \end{bmatrix} \begin{bmatrix} \delta\boldsymbol{\varphi}_I \\ \delta\boldsymbol{t}_I \\ \delta\lambda_I \end{bmatrix} \tag{A.1}$$

with $l^I_\alpha = N^I_{,\alpha}\lambda + N^I\lambda_{,\alpha}$ and $\boldsymbol{m}^I_\alpha = N^I_{,\alpha}\boldsymbol{t} + N^I\boldsymbol{t}_{,\alpha}$. Due to the assumed interpolation (53) of the transverse shear strains, the contribution to the operator matrix (55) is obtained from

$$\begin{bmatrix} 2\delta\hat{E}_{13} \\ 2\delta\hat{E}_{23} \end{bmatrix} = \begin{bmatrix} \boldsymbol{B}^S_\varphi & \boldsymbol{B}^S_t & \boldsymbol{B}^S_\lambda \end{bmatrix} \begin{bmatrix} \delta\boldsymbol{\varphi}_K \\ \delta\boldsymbol{t}_K \\ \delta\boldsymbol{\lambda}_K \end{bmatrix} \quad \text{where} \quad \begin{aligned} \delta\boldsymbol{\varphi}_K &= [\delta\boldsymbol{\varphi}_1, \ \delta\boldsymbol{\varphi}_2, \ \delta\boldsymbol{\varphi}_3, \ \delta\boldsymbol{\varphi}_4] \\ \delta\boldsymbol{t}_K &= [\delta\boldsymbol{t}_1, \ \delta\boldsymbol{t}_2, \ \delta\boldsymbol{t}_3, \ \delta\boldsymbol{t}_4] \\ \delta\boldsymbol{\lambda}_K &= [\delta\lambda_1, \ \delta\lambda_2, \ \delta\lambda_3, \ \delta\lambda_4] \end{aligned} \tag{A.2}$$

and the submatrices are defined by

$$\boldsymbol{B}^S_\varphi = \frac{1}{4}\begin{bmatrix} -(1-\eta)\boldsymbol{d}_B^{\mathrm{T}} & (1-\eta)\boldsymbol{d}_B^{\mathrm{T}} & (1+\eta)\boldsymbol{d}_D^{\mathrm{T}} & -(1+\eta)\boldsymbol{d}_D^{\mathrm{T}} \\ -(1-\xi)\boldsymbol{d}_A^{\mathrm{T}} & -(1+\xi)\boldsymbol{d}_C^{\mathrm{T}} & (1+\xi)\boldsymbol{d}_C^{\mathrm{T}} & (1-\xi)\boldsymbol{d}_A^{\mathrm{T}} \end{bmatrix} \tag{A.3}$$

$$\boldsymbol{B}^S_t = \frac{1}{4}\begin{bmatrix} (1-\eta)\lambda^B\boldsymbol{\varphi}_{,1}^{B\mathrm{T}} & (1-\eta)\lambda^B\boldsymbol{\varphi}_{,1}^{B\mathrm{T}} & (1+\eta)\lambda^D\boldsymbol{\varphi}_{,1}^{D\mathrm{T}} & (1+\eta)\lambda^D\boldsymbol{\varphi}_{,1}^{D\mathrm{T}} \\ (1-\xi)\lambda^A\boldsymbol{\varphi}_{,2}^{A\mathrm{T}} & (1+\xi)\lambda^C\boldsymbol{\varphi}_{,2}^{C\mathrm{T}} & (1+\xi)\lambda^C\boldsymbol{\varphi}_{,2}^{C\mathrm{T}} & (1-\xi)\lambda^A\boldsymbol{\varphi}_{,2}^{A\mathrm{T}} \end{bmatrix} \tag{A.4}$$

$$\boldsymbol{B}^S_\lambda = \frac{1}{4}\begin{bmatrix} (1-\eta)(\boldsymbol{\varphi}_{,1}^{B\mathrm{T}}\boldsymbol{t}^B - \xi^3\lambda_1) & (1-\eta)(\boldsymbol{\varphi}_{,1}^{B\mathrm{T}}\boldsymbol{t}^B + \xi^3\lambda_2) \\ (1-\xi)(\boldsymbol{\varphi}_{,2}^{A\mathrm{T}}\boldsymbol{t}^A - \xi^3\lambda_1) & (1+\xi)(\boldsymbol{\varphi}_{,2}^{C\mathrm{T}}\boldsymbol{t}^C - \xi^3\lambda_2) \\ (1+\eta)(\boldsymbol{\varphi}_{,1}^{D\mathrm{T}}\boldsymbol{t}^D + \xi^3\lambda_3) & (1+\eta)(\boldsymbol{\varphi}_{,1}^{D\mathrm{T}}\boldsymbol{t}^D - \xi^3\lambda_4) \\ (1+\xi)(\boldsymbol{\varphi}_{,2}^{C\mathrm{T}}\boldsymbol{t}^C + \xi^3\lambda_3) & (1-\xi)(\boldsymbol{\varphi}_{,2}^{A\mathrm{T}}\boldsymbol{t}^A + \xi^3\lambda_4) \end{bmatrix}. \tag{A.5}$$

A.2. Geometric part of the tangent stiffness matrix

The geometric part of the element tangent operator follows from the discrete internal virtual work expression (54)

$$G^{\mathrm{int}}_e = \int_{B^h_0} \hat{\boldsymbol{S}} \cdot \delta\boldsymbol{E}\, \mathrm{d}V = \int_{B^h_0} \left[\hat{S}^{\alpha\beta}\,\delta E_{\alpha\beta} + \hat{S}^{33}\,\delta E_{33} + 2\hat{S}^{\alpha 3}\,\delta\hat{E}_{\alpha 3}\right] \mathrm{d}V \tag{A.6}$$

by linearization of the configuration holding the stress components $\hat{S}^{IJ}$ fixed. Employing the shell kinematics one obtains for the tangential part

$$\hat{S}^{\alpha\beta}\,\delta E_{\alpha\beta} = \hat{S}^{\alpha\beta}[(\delta\boldsymbol{\varphi}_{,\alpha} + \xi^3\,\delta\boldsymbol{d}_{,\alpha})\cdot\boldsymbol{x}_{,\beta}] \tag{A.7}$$

and for the thickness part

$$\hat{S}^{33}\,\delta E_{33} = \hat{S}^{33}\lambda\,\delta\lambda\,. \tag{A.8}$$

Using the interpolation formulas of Section 4.1 yields the discrete tangential part

$$\hat{S}^{\alpha\beta}\,\delta E_{\alpha\beta} = \sum_{I=1}^{4} \hat{S}^{\alpha\beta}\left[N^I_{,\alpha}\boldsymbol{x}^{\mathrm{T}}_{,\beta}\,\delta\boldsymbol{\varphi}_I + \xi^3(N^I_{,\alpha}\lambda + N^I\lambda_{,\alpha})\boldsymbol{x}^{\mathrm{T}}_{,\beta}\,\delta\boldsymbol{t}_I + \xi^3(N^I_{,\alpha}\boldsymbol{t}^{\mathrm{T}} + N^I\boldsymbol{t}^{\mathrm{T}}_{,\alpha})\boldsymbol{x}_{,\beta}\,\delta\lambda_I\right] \tag{A.9}$$

and the discrete thickness part

$$\hat{S}^{33}\,\delta E_{33} = \hat{S}^{33}\lambda\sum_{I=1}^{4} N^I\,\delta\lambda_I \tag{A.10}$$

so that the tangential and thickness contribution to the geometric stiffness matrix $\boldsymbol{G}_{IJ}$ (61) is given by

$$\begin{aligned}
&\hat{S}^{\alpha\beta}\,\Delta\delta E_{\alpha\beta} + \hat{S}^{33}\,\Delta\delta E_{33}\\
&= \sum_{I=1}^{4}\sum_{J=1}^{4} \delta\boldsymbol{\varphi}_I^{\mathrm{T}}(\hat{S}^{\alpha\beta}N^I_{,\alpha}N^J_{,\beta})\,\Delta\boldsymbol{\varphi}_J\\
&\quad + \sum_{I=1}^{4}\sum_{J=1}^{4}\Big[\ \delta\boldsymbol{\varphi}_I^{\mathrm{T}}(\hat{S}^{\alpha\beta}\xi^3N^I_{,\alpha}l^J_{\beta}\ \mathbf{1})\,\Delta\boldsymbol{t}_J + \delta\boldsymbol{t}_I^{\mathrm{T}}(\hat{S}^{\alpha\beta}\xi^3N^J_{,\beta}l^I_{\alpha}\ \mathbf{1})\,\Delta\boldsymbol{\varphi}_J\Big]\\
&\quad + \sum_{I=1}^{4}\sum_{J=1}^{4}\delta\boldsymbol{t}_I^{\mathrm{T}}[\hat{S}^{\alpha\beta}(\xi^3)^2l^I_{\alpha}l^J_{\beta}\ \mathbf{1}]\,\Delta\boldsymbol{t}_J - \sum_{I=1}^{4}\delta\boldsymbol{t}_I^{\mathrm{T}}[\hat{S}^{\alpha\beta}\xi^3l^I_{\alpha}(\boldsymbol{x}^{\mathrm{T}}_{,\beta}\boldsymbol{t}_I)\ \mathbf{1}]\,\Delta\boldsymbol{t}_I\\
&\quad + \sum_{I=1}^{4}\sum_{J=1}^{4}\Big[\ \delta\boldsymbol{\varphi}_I^{\mathrm{T}}(\hat{S}^{\alpha\beta}\xi^3N^I_{,\alpha}\boldsymbol{m}^J_{\beta})\,\Delta\lambda_J + \delta\lambda_I(\hat{S}^{\alpha\beta}\xi^3N^J_{,\beta}\boldsymbol{m}^{I\mathrm{T}}_{\alpha})\,\Delta\boldsymbol{\varphi}_J\Big]\\
&\quad + \sum_{I=1}^{4}\sum_{J=1}^{4}\Big[\ \delta\boldsymbol{t}_I^{\mathrm{T}}[\hat{S}^{\alpha\beta}(\xi^3n^{IJ}_{\alpha}\boldsymbol{x}_{,\beta} + (\xi^3)^2l^I_{\alpha}\boldsymbol{m}^J_{\beta})]\,\Delta\lambda_J + \delta\lambda_I[\hat{S}^{\alpha\beta}(\xi^3n^{IJ}_{\alpha}\boldsymbol{x}^{\mathrm{T}}_{,\beta} + (\xi^3)^2l^I_{\beta}\boldsymbol{m}^{I\mathrm{T}}_{\alpha})]\,\Delta\boldsymbol{t}_J\Big]\\
&\quad + \sum_{I=1}^{4}\sum_{J=1}^{4}\delta\lambda_I[\hat{S}^{33}N^IN^J + \hat{S}^{\alpha\beta}(\xi^3)^2(N^I_{,\alpha}N^J_{,\beta} + N^IN^J\boldsymbol{t}^{\mathrm{T}}_{,\alpha}\boldsymbol{t}_{,\beta})]\,\Delta\lambda_J
\end{aligned} \tag{A.11}$$

where the following abbreviations have been used

$$l^J_{\alpha} = N^J_{,\alpha}\lambda + N^J\lambda_{,\alpha}, \qquad \boldsymbol{m}^I_{\alpha} = N^J_{,\alpha}\boldsymbol{t} + N^J\boldsymbol{t}_{,\alpha} \quad \text{and} \quad n^{IJ}_{\alpha} = N^I_{,\alpha}N^J + N^IN^J_{,\alpha}. \tag{A.12}$$

Due to the assumed shear strain approach one obtains the contribution to the geometric stiffness matrix $\boldsymbol{G}_{IJ}$ (61)

$$\begin{aligned}
2\hat{S}^{\alpha 3}\,\Delta\delta\hat{E}_{\alpha 3} = {}& \delta\boldsymbol{\varphi}_K^{\mathrm{T}}\boldsymbol{A}\,\Delta\boldsymbol{t}_K + \delta\boldsymbol{t}_K\boldsymbol{A}^{\mathrm{T}}\,\Delta\boldsymbol{\varphi}_K + \delta\boldsymbol{\varphi}_K^{\mathrm{T}}\boldsymbol{B}\,\Delta\boldsymbol{\lambda}_K + \delta\boldsymbol{\lambda}_K^{\mathrm{T}}\boldsymbol{B}^{\mathrm{T}}\,\Delta\boldsymbol{\varphi}_K\\
&+\delta\boldsymbol{t}_K^{\mathrm{T}}\boldsymbol{C}\,\Delta\boldsymbol{\lambda}_K + \delta\boldsymbol{\lambda}_K^{\mathrm{T}}\boldsymbol{C}^{\mathrm{T}}\,\Delta\boldsymbol{t}_K + \delta\boldsymbol{t}_K^{\mathrm{T}}\boldsymbol{D}\,\Delta\boldsymbol{t}_K + \delta\boldsymbol{\lambda}_K^{\mathrm{T}}\boldsymbol{E}\,\Delta\boldsymbol{\lambda}_K
\end{aligned} \tag{A.13}$$

where $\boldsymbol{\varphi}_K$, $\boldsymbol{t}_K$ and $\boldsymbol{\lambda}_K$ denote the nodal vectors defined in (A.2). Moreover we make use of the following matrices

$$\boldsymbol{A} = \begin{bmatrix} -(A+B)\,\mathbf{1} & -B\,\mathbf{1} & \mathbf{0} & -A\,\mathbf{1}\\ B\,\mathbf{1} & (B-C)\,\mathbf{1} & -C\,\mathbf{1} & \mathbf{0}\\ \mathbf{0} & C\,\mathbf{1} & (C+D)\,\mathbf{1} & D\,\mathbf{1}\\ A\,\mathbf{1} & \mathbf{0} & -D\,\mathbf{1} & (A-D)\,\mathbf{1} \end{bmatrix} \qquad \boldsymbol{B} = \begin{bmatrix} -(\boldsymbol{a}+\boldsymbol{b}) & -\boldsymbol{b} & \mathbf{0} & -\boldsymbol{a}\\ \boldsymbol{b} & \boldsymbol{b}-\boldsymbol{c} & -\boldsymbol{c} & \mathbf{0}\\ \mathbf{0} & \boldsymbol{c} & \boldsymbol{c}+\boldsymbol{d} & \boldsymbol{d}\\ \boldsymbol{a} & \mathbf{0} & -\boldsymbol{d} & \boldsymbol{a}-\boldsymbol{d} \end{bmatrix}$$

$$\boldsymbol{C} = \begin{bmatrix} \boldsymbol{\alpha}+\boldsymbol{\beta} & \boldsymbol{\beta} & \mathbf{0} & \boldsymbol{\alpha}\\ \boldsymbol{\beta} & \boldsymbol{\beta}+\boldsymbol{\gamma} & \boldsymbol{\gamma} & \mathbf{0}\\ \mathbf{0} & \boldsymbol{\gamma} & \boldsymbol{\gamma}+\boldsymbol{\delta} & \boldsymbol{\delta}\\ \boldsymbol{\alpha} & \mathbf{0} & \boldsymbol{\delta} & \boldsymbol{\alpha}+\boldsymbol{\delta} \end{bmatrix} \qquad \boldsymbol{D} = \operatorname{diag}[(a_1+b_1)\,\mathbf{1},\ (b_2+c_2)\,\mathbf{1},\ (c_3+d_3)\,\mathbf{1},\ (a_4+d_4)\,\mathbf{1}]$$

$$\boldsymbol{E} = \xi^3\operatorname{diag}[-(a+b),\ b-c,\ (c+d),\ a-d]$$

with the abbreviations

$$a = \frac{1}{4}(1-\xi)\hat{S}^{23} \qquad A = \frac{1}{2}a\lambda^A \qquad \boldsymbol{a} = \frac{1}{2}a\boldsymbol{t}^A \qquad \boldsymbol{\alpha} = \frac{1}{2}a\boldsymbol{\varphi}^A_{,2}$$

$$b = \frac{1}{4}(1-\eta)\hat{S}^{13} \qquad B = \frac{1}{2}b\lambda^B \qquad \boldsymbol{b} = \frac{1}{2}b\boldsymbol{t}^B \qquad \boldsymbol{\beta} = \frac{1}{2}b\boldsymbol{\varphi}^B_{,1}$$

$$c = \frac{1}{4}(1+\xi)\hat{S}^{23} \qquad C = \frac{1}{2}c\lambda^{C} \qquad \boldsymbol{c} = \frac{1}{2}c\boldsymbol{t}^{C} \qquad \boldsymbol{\gamma} = \frac{1}{2}c\boldsymbol{\varphi}^{C}_{,2}$$

$$d = \frac{1}{4}(1+\eta)\hat{S}^{13} \qquad D = \frac{1}{2}d\lambda^{D} \qquad \boldsymbol{d} = \frac{1}{2}d\boldsymbol{t}^{D} \qquad \delta = \frac{1}{2}d\boldsymbol{\varphi}^{D}_{,1}$$

$$a_1 = -a\lambda^{A}\boldsymbol{t}_1^{\mathrm{T}}\boldsymbol{\varphi}^{A}_{,2} \qquad b_1 = -b\lambda^{B}\boldsymbol{t}_1^{\mathrm{T}}\boldsymbol{\varphi}^{B}_{,1} \qquad c_2 = -c\lambda^{C}\boldsymbol{t}_2^{\mathrm{T}}\boldsymbol{\varphi}^{C}_{,2} \qquad d_3 = -\mathrm{d}\lambda^{D}\boldsymbol{t}_3^{\mathrm{T}}\boldsymbol{\varphi}^{D}_{,1}$$

$$a_4 = -a\lambda^{A}\boldsymbol{t}_4^{\mathrm{T}}\boldsymbol{\varphi}^{A}_{,2} \qquad b_2 = -b\lambda^{B}\boldsymbol{t}_2^{\mathrm{T}}\boldsymbol{\varphi}^{B}_{,1} \qquad c_3 = -c\lambda^{C}\boldsymbol{t}_3^{\mathrm{T}}\boldsymbol{\varphi}^{C}_{,2} \qquad d_4 = -\mathrm{d}\lambda^{D}\boldsymbol{t}_4^{\mathrm{T}}\boldsymbol{\varphi}^{D}_{,1}$$

A.3. Constitutive laws

This appendix summarizes the complete, unmodified 3d hyperelastic constitutive laws used in the numerical simulations. The second Piola–Kirchhoff stress tensor $\hat{\boldsymbol{S}}$ and the constitutive relation tensor $\hat{\boldsymbol{C}}$ are obtained from the strain energy density function $\hat{W}_{0\mathrm{v}}$ per unit initial volume by

$$\hat{\boldsymbol{S}} = \frac{\partial \hat{W}_{0\mathrm{v}}}{\partial \boldsymbol{E}} \quad \text{and} \quad \hat{\boldsymbol{C}} = \frac{\partial^2 \hat{W}_{0\mathrm{v}}}{\partial \boldsymbol{E}\,\partial \boldsymbol{E}}. \tag{A.14}$$

Applying the covariant Green–Lagrangian strains requires the stress and constitutive tensors to be referred to the covariant basis of the reference configuration

$$\hat{\boldsymbol{S}} = \hat{S}^{ij}\boldsymbol{G}_i \otimes \boldsymbol{G}_j \quad \text{and} \quad \hat{\boldsymbol{C}} = \hat{C}^{ijkl}\boldsymbol{G}_i \otimes \boldsymbol{G}_j \otimes \boldsymbol{G}_k \otimes \boldsymbol{G}_l. \tag{A.15}$$

Moreover, the components of the right Cauchy–Green deformation tensor

$$\boldsymbol{C} = g_{ij}\boldsymbol{G}^i \otimes \boldsymbol{G}^j \tag{A.16}$$

are given by

$$\begin{aligned} g_{\alpha\beta} &= g^{C}_{\alpha\beta} + 2\tilde{E}_{\alpha\beta} \\ g_{33} &= \lambda^2 + 2\tilde{E}_{33} \\ g_{\alpha 3} &= G_{\alpha 3} + 2\hat{E}_{\alpha 3} \end{aligned} \tag{A.17}$$

where g^{C}_{ij} denote the compatible metric coefficients (14). In the sequel I_1 and I_2 denote the invariants of the right Cauchy–Green deformation tensor $\boldsymbol{C}$, further $J = \sqrt{g/G}$, μ and λ the Lamé constants.

- St. Venant-Kirchhoff model:

$$\begin{aligned} &\hat{W}_{0\mathrm{v}} = \frac{\lambda}{2}(\mathrm{tr}\,\boldsymbol{E})^2 + \mu\,\mathrm{tr}\,\boldsymbol{E}^2 \\ &\hat{\boldsymbol{S}} = \lambda\,\mathrm{tr}\,\boldsymbol{E}\,\boldsymbol{1} + 2\mu\boldsymbol{E} \\ &\hat{\boldsymbol{C}} = \lambda\,\boldsymbol{1}\otimes\boldsymbol{1} + 2\mu\,\boldsymbol{1} \\ &\hat{S}^{ij} = \frac{\lambda}{2}(G^{kl}g_{kl} - 3)G^{ij} + \mu(G^{ik}g_{kl}G^{lj} - G^{ij}) = \hat{C}^{ijkl}E_{kl} \\ &\hat{C}^{ijkl} = \lambda G^{ij}G^{kl} + \mu(G^{ik}G^{jl} + G^{jk}G^{il}) \end{aligned} \tag{A.18}$$

- Compressible Neo-Hooke model:

$$\begin{aligned} &\hat{W}_{0\mathrm{v}} = \frac{\mu}{2}(J^{-2/3}I_1 - 3) + U(J), \quad U(J) = K\left(\frac{1}{2}(J^2-1) - \ln J\right) \\ &\hat{\boldsymbol{S}} = \mu J^{-2/3}\,\boldsymbol{1} + \left(JU' - \frac{1}{3}\mu J^{-2/3}I_1\right)\boldsymbol{C}^{-1} \\ &\hat{\boldsymbol{C}} = -\frac{2}{3}\mu J^{-2/3}\boldsymbol{C}^{-1}\otimes\boldsymbol{1} + \boldsymbol{1}\otimes\boldsymbol{C}^{-1} + \left(\frac{2}{9}\mu J^{-2/3}I_1 + J^2U'' + JU'\right)\boldsymbol{C}^{-1}\otimes\boldsymbol{C}^{-1} \\ &\qquad + \left(-\frac{2}{3}\mu J^{-2/3}I_1 + 2JU'\right)\frac{\partial \boldsymbol{C}^{-1}}{\partial \boldsymbol{C}} \end{aligned} \tag{A.19}$$

$$\hat{S}^{ij} = \mu J^{-2/3} G^{ij} + (J U' - \frac{1}{3}\mu J^{-2/3} G^{kl} g_{kl}) g^{ij}$$

$$\hat{C}^{ijkl} = -\frac{2}{3}\mu J^{-2/3}(g^{ij}G^{kl} + G^{ij}g^{kl}) + \left(\frac{2}{9}\mu J^{-2/3} G^{mn} g_{mn} + J^2 U'' + J U'\right) g^{ij} g^{kl} + \left(\frac{1}{3}\mu J^{-2/3} G^{mn} g_{mn} - J U'\right)(g^{ik} g^{jl} + g^{jk} g^{il})$$

- Compressible Mooney–Rivlin model:

$$\hat{W}_{0s} = c_1(I_1 - 3) + c_2(I_2 - 3) + U(J),$$
$$U(J) = \frac{\varepsilon}{2}(\ln J)^2 - 2(c_1 + 2c_2)\ln J + \gamma \ln J \tag{A.20}$$

$U(J)$ denotes the extension to the compressible range of the constitutive model for the incompressible material. The incompressibility constraint $J = 1$ is enforced by the augmented Lagrangian method. Accordingly ε serves as a penalty parameter and γ denotes the augmented Lagrangian multiplier.

$$\hat{\boldsymbol{S}} = 2(c_1 + c_2 I_1)\,\mathbf{1} - 2c_2 \boldsymbol{C} + (\varepsilon \ln J + \gamma - 2(c_1 + 2c_2))\boldsymbol{C}^{-1}$$
$$\hat{\boldsymbol{C}} = 4c_2\,\mathbf{1} \otimes \mathbf{1} - 4c_2\,\mathbf{1} + 2(\varepsilon \ln J + \gamma - 2(c_1 + 2c_2))\frac{\partial \boldsymbol{C}^{-1}}{\partial \boldsymbol{C}} + \varepsilon \boldsymbol{C}^{-1} \otimes \boldsymbol{C}^{-1}$$
$$\hat{S}^{ij} = 2(c_1 + c_2 G^{kl} g_{kl}) G^{ij} - 2c_2 G^{ik} g_{kl} G^{lj} + (\varepsilon \ln J + \gamma - 2(c_1 + 2c_2)) g^{ij} \tag{A.21}$$
$$\hat{C}^{ijkl} = 4c_2 G^{ij} G^{kl} - 2c_2(G^{ik} G^{jl} + G^{jk} G^{il}) + \varepsilon g^{ij} g^{kl} - (\varepsilon \ln J + \gamma - 2(c_1 + 2c_2))(g^{ik} g^{jl} + g^{jk} g^{il})$$

The coefficients $\hat{C}^{ijkl}$ are subsequently arranged in the matrix $[\hat{C}^{ijkl}] \in \mathbb{R}^{6\times 6}$ according to the ordering of the strain and stress components (51) and (57).

References

[1] E. Ramm, Geometrisch nichtlineare Elastostatik und finite Elemente, Habilitation, Bericht Nr. 76-2, Institut für Baustatik, Universität Stuttgart, 1976.

[2] J.H. Argyris, P.C. Dunne, G.A. Malejannakis and E. Schelkle, A simple triangular facet shell element with applications to linear and non-linear equilibrium and elastic stability problems, Comput. Methods Appl. Mech. Engrg. 10 (1977) 371–403.

[3] F. Gruttmann, E. Stein and P. Wriggers, Theory and numerics of thin elastic shells with finite rotations, Ingenieur-Archiv 59 (1989) 54–67.

[4] J.C. Simo, D.D. Fox and M.S. Rifai, On a stress resultant geometrically exact shell model. Part III: Computational aspects of the non-linear theory, Comput. Methods Appl. Mech. Engrg. 79 (1990) 21–70.

[5] Y. Basar, Y. Ding and W.B. Krätzig, Finite-rotatation shell elements via mixed formulation, Comput. Mech. 10 (1992) 289–306.

[6] C. Sansour and H. Bufler, An exact finite rotation shell theory, its mixed variational formulation and its finite element implementation, Int. J. Numer. Methods Engrg. 31 (1992) 73–115.

[7] P. Wriggers and F. Gruttmann, Thin shells with finite rotations formulated in biot-stresses: Theory and finite element formulation, Int. J. Numer. Methods Engrg. 36 (1993) 2049–2071.

[8] E. Stein, B. Seifert, S. Ohnimus and C. Carstensen, Adaptive finite element analysis of geometrically non-linear plates and shells, especially buckling, Int. J. Numer. Methods Engrg. 37 (1994) 2631–2655.

[9] T.J.R. Hughes and E. Carnoy, Non-linear finite element shell formulation accounting for large membrane strains, Comput. Methods Appl. Mech. Engrg. 39 (1983) 69–82.

[10] H. Parisch, Efficient non-linear finite element shell formulation involving large strains, Engrg. Comput. 3 (1986) 121–128.

[11] B. Schieck, W. Pietraszkiewicz and H. Stumpf, Theory and numerical analysis of shells undergoing large elastic strains, Int. J. Solids Struct. 29(6) (1992) 689–709.

[12] H. Schoop, Oberflächenorientierte Schalentheorien endlicher Verschiebungen, Ingenieur-Archiv 56 (1986) 427–437.

[13] B. A. Szabó and G. J. Sahrmann, Hierarchic plate and shell models based on p-extension, Int. J. Numer. Methods Engrg. 26 (1988) 1855–1881.

[14] N. Büchter, E. Ramm and D. Roehl, Three-dimensional extension of non-linear shell formulations based on the enhanced assumed strain concept, Int. J. Numer. Methods Engrg. 37 (1994) 2551–2568.

[15] J.C. Simo, M.S. Rifai and D.D. Fox, On a stress resultant geometrically exact shell model. Part IV: Variable thickness shells with through-the-thickness stretching, Comput. Methods Appl. Mech. Engrg. 81 (1990) 91–126.

[16] J.G. Simmonds, The strain energy density of rubber-like shells, Int. J. Solids Struct. 21(1) (1985) 67–77.

[17] H. Stumpf and J. Makowski, On large strain deformations of shells, Acta Mechanica 65 (1986) 153–168.

[18] J.C. Simo and M.S. Rifai, A class of mixed assumed strain methods and the method of incompatible modes, Int. J. Numer. Methods Engrg. 29 (1990) 1595–1638.

[19] J.C. Simo and F. Armero, Geometrically non-linear enhanced strain mixed methods and the method of incompatible modes, Int. J. Numer. Methods Engrg. 33 (1992) 1413–1449.
[20] B.D. Reddy and J.C. Simo, Stability and convergence of a class of enhanced strain methods, Preprint (1994).
[21] T.J.R. Hughes and W.K. Liu, Non-linear finite element analysis of shells: Part I. Three-dimensional shells, Comput. Methods Appl. Mech. Engrg. 26 (1981) 331–362.
[22] J.C. Simo, On a stress resultant geometrically exact shell model. Part VII: Shell intersections with 5/6-DOF finite element formulations, Comput. Methods Appl. Mech. Engrg. 108 (1993) 319–339.
[23] H. Parisch, An investigation of a finite rotation four node assumed strain shell element, Int. J. Numer. Methods Engrg. 31 (1991) 127–150.
[24] J. Argyris, An excursion into large rotations, Comput. Methods Appl. Mech. Engrg. 32 (1982) 85–155.
[25] N. Büchter and E. Ramm, Shell theory versus degeneration—A comparison in large rotation finite element analysis, Int. J. Numer. Methods Engrg. 34 (1992) 39–59.
[26] B. Szabó and I. Babuška, Finite Element Analysis (John Wiley & Sons, New York, 1991).
[27] U. Andelfinger and E. Ramm, EAS-elements for two-dimensional, three-dimensional, plate and shell structures and their equivalence to HR-elements, Int. J. Numer. Methods Engrg. 36 (1993) 1311–1337.
[28] E.N. Dvorkin and K.-J. Bathe, A continuum mechanics based four-node shell element for general non-linear analysis, Engrg. Comput. 1 (1984) 77–88.
[29] O.C. Zienkiewicz and R.L. Taylor, The Finite Element Method, 4th edition, Volume 1 (McGraw Hill, London, 1988).
[30] W. Wagner and F. Gruttmann, A simple finite rotation formulation for composite shell elements, Engrg. Comput. 11 (1994) 145–176.
[31] R.H. MacNeal and R.L. Harder, A proposed standard set of problems to test finite element accuracy, Finite Elements Anal. Des. 1 (1985) 3–20.
[32] J. Chroscielewski, J. Makowski and H. Stumpf, Genuinely resultant shell finite elements accounting for geometric and material non-linearity, Int. J. Numer. Methods Engrg. 35 (1992) 63–94.
[33] F. Gruttmann and R.L. Taylor, Theory and finite element formulation of rubberlike membrane shells using principal stretches, Int. J. Numer. Methods Engrg. 35 (1992) 1111–1126.
[34] C. Miehe, Aspects of the formulation and finite element implementation of large strain isotropic elasticity, Int. J. Numer. Methods Engrg. 37 (1994) 1981–2004.